18F-Fluorocholine PET uptake correlates with pathologic evidence of recurrent tumor after stereotactic radiosurgery for brain metastases

Milan Grkovski[1], **Zachary A. Kohutek**[2,*], **Heiko Schöder**[3,4], **Cameron W. Brennan**[5,6], **Viviane S. Tabar**[5], **Philip H. Gutin**[5], **Zhigang Zhang**[7], **Robert J. Young**[3], **Bradley J. Beattie**[1], **Pat B. Zanzonico**[1], **Jason T. Huse**[6,8,†], **Marc K. Rosenblum**[8], **Ronald G. Blasberg**[3,9,10], **John L. Humm**[1], **Kathryn Beal**[2]

[1]Department of Medical Physics, Memorial Sloan Kettering Cancer Center, New York, NY

[2]Department of Radiation Oncology, Memorial Sloan Kettering Cancer Center, New York, NY

[3]Department of Radiology, Memorial Sloan Kettering Cancer Center, New York, NY

[4]Molecular Imaging and Therapy Service, Memorial Sloan Kettering Cancer Center, New York, NY

[5]Department of Neurosurgery, Memorial Sloan Kettering Cancer Center, New York, NY

[6]Human Oncology and Pathogenesis Program, Memorial Sloan Kettering Cancer Center, New York, NY

[7]Department of Epidemiology & Biostatistics, Memorial Sloan Kettering Cancer Center, New York, NY

[8]Department of Pathology, Memorial Sloan Kettering Cancer Center, New York, NY

[9]Department of Neurology, Memorial Sloan Kettering Cancer Center, New York, NY

[10]Molecular Pharmacology Program, Memorial Sloan Kettering Cancer Center, New York, NY

Abstract

Purpose: Radiographic changes of brain metastases after stereotactic radiosurgery (SRS) can signify tumor recurrence and/or radiation necrosis (RN), however standard imaging modalities cannot easily distinguish between these two entities. We investigated whether ^{18}F-Fluorocholine

Corresponding Author: Kathryn Beal, MD, Department of Radiation Oncology, Memorial Sloan Kettering Cancer Center, 1275 York Avenue, New York, NY 10065, Phone: 212-639-5159, bealk@mskcc.org.
*Current address: Department of Radiation Oncology, Vanderbilt University Medical Center, Nashville, TN
†Current address: Pathology Department, MD Anderson Cancer Center, Houston, TX

uptake in surgical samples of the resected lesions correlates with pathologic evidence of recurrent tumor and PET imaging.

Methods: 14 patients previously treated with SRS that developed radiographic changes were included. All patients underwent a pre-operative 40-min dynamic PET/CT concurrent with 392±11 MBq bolus injection of ^{18}F-Fluorocholine. ^{18}F-Fluorocholine pharmacokinetics were evaluated by standardized uptake value (SUV), graphical analysis (Patlak plot; K_i^P) and an irreversible 2-compartment model (K_1, k_2, k_3 and K_i). 12 out of 14 patients were administered an additional 72±14 MBq injection of ^{18}F-Fluorocholine 95±26 minutes prior to surgical resection. 113 resected samples from 12 patients were blindly reviewed by a neuropathologist to assess the viable tumor and necrotic content, microvascular proliferation, reactive gliosis and mono- and polymorphonuclear inflammatory infiltrates. Correlation between these metrics ^{18}F-Fluorocholine SUV was investigated with a linear mixed model. Comparison of survival distributions of two groups of patients (population median split of PET SUV_{max}) was performed with the log-rank test.

Results: 10 out of 12 patients for which surgical samples were acquired exhibited pathologic recurrence. Strong correlation was observed between SUV_{max} as measured from a surgically removed sample with highest uptake and by PET (Pearson's r=0.66). Patients with ^{18}F-Fluorocholine PET SUV_{max} >6 experienced poor survival. Surgical samples with viable tumor had higher ^{18}F-fluorocholine uptake (SUV) than those without tumor (4.5±3.7 and 2.6±3.0; p=0.01). ^{18}F-fluorocholine count data from surgical samples is driven not only by the percentage viable tumor, but also by the degree of inflammation and reactive gliosis. (p 0.02; multivariate regression).

Conclusions: ^{18}F-Fluorocholine accumulation is increased in viable tumor, however inflammation and gliosis may also lead to elevated uptake. Higher ^{18}F-Fluorocholine PET uptake portends worse prognosis. Kinetic analysis of dynamic ^{18}F-Fluorocholine PET imaging supports the adequacy of the simpler static SUV metric.

INTRODUCTION

The incidence of brain metastases (BM) has been rising due to improved imaging techniques, which aid early diagnosis, and systemic therapies which prolong life [1]. Stereotactic radiosurgery (SRS) is an effective treatment for patients with a limited number of BM. Its advantages over surgery and whole brain radiation therapy include short treatment time and limited side effects that allow preservation of quality of life. Up to 40% of BM treated with SRS will eventually develop either radionecrosis (RN) or tumor recurrence [2]. These two entities can occur within the same time interval after SRS with similar frequency [1,3] and have similar architectural appearance on a magnetic resonance imaging (MRI) scan. Both result in similar symptoms (such as headaches, cognitive or motor difficulties and seizures), but they require different therapeutic management and impact prognosis differently. RN can often be managed conservatively, reducing the need for surgical intervention and associated risk, whereas tumor recurrence needs to be managed

with surgery, repeat radiation, and possibly systemic agents. Standard imaging techniques such as MRI perfusion, MR spectroscopy or ^{18}F-Fluorodeoxyglucose (^{18}F-FDG) positron emission tomography/computed tomography (PET/CT) cannot easily distinguish between these two entities.

The current reference standard for distinguishing tumor recurrence from radionecrosis is biopsy, where conclusive histopathologic diagnosis is achieved in >99% of cases [4]. However, biopsy is invasive and has potential complications such as transient or permanent neurological deficits [5]. Furthermore, many treated BM are in deep or eloquent locations that are not amenable to biopsy. There is a need for a reliable non-invasive imaging technique enabling the accurate differentiation of recurrent tumor from radionecrosis

Choline is a precursor of phospholipids, major structural components of the plasma membrane, and is frequently overexpressed in malignancies [6]. It is predominantly transported into cells via high-affinity sodium dependent choline transporters, phosphorylated by choline kinase and utilized for the synthesis of essential lipid components of cell membranes (e.g., phosphatidylcholine and sphingomyelin), the production of potent lipid mediators (such as platelet-activation factor and lysophosphatidylcholine) and the synthesis of the cholinergic neurotransmitter acetylcholine. Intracellular choline is rapidly metabolized to phosphocholine or oxidized by choline dehydrogenase and betaine-aldehyde dehydrogenase to betaine. ^{18}F-Fluorocholine, a 18 F-substituted choline analog, is rapidly cleared from the circulation, with previous studies indicating that its biodistribution changes very slowly after 10-min post-injection [7]. Kwee and colleagues reported that high-grade gliomas, BM and benign lesions can be distinguished based on their ^{18}F-Fluorocholine uptake [8].

We hypothesized that PET imaging with ^{18}F-Fluorocholine would reliably discriminate between RN and tumor recurrence. For that purpose, we performed ^{18}F-Fluorocholine dynamic PET scans in patients with radiographic changes requiring surgery after SRS for BM. PET-derived imaging metrics were subsequently compared with the level of ^{18}F-Fluorocholine radioactivity in tissue samples resected from the lesion and for which a detailed histopathologic assessment was available. We also explored whether pharmacokinetic modeling of dynamic ^{18}F-Fluorocholine PET data provided added benefit.

METHODS AND MATERIALS

Study design and patient selection

A prospective non-therapeutic trial was performed with ^{18}F-Fluorocholine PET imaging in patients with recurrent tumor and/or RN following SRS for BM. Human use of ^{18}F-Fluorocholine was approved by our Institutional Radioactive Drug Research Council (RDRC). The RDRC rules permit research studies to be performed with novel radiotracers without an investigational new drug designation. The protocol was approved by the Institutional Review Board (Protocol # 13–199; registered under ClinicalTrials.gov Identifier NCT02037945), and all patients provided written informed consent regarding the examination and use of anonymous data for research and publication purposes. The trial was intended to investigate the localization of ^{18}F-Fluorocholine within the irradiated brain using

a PET/CT and was not used to assess treatment response or to change treatment decisions. The study enrolled patients who were scheduled to undergo surgical resection. Patients were also administered a second dose of ^{18}F-Fluorocholine in the operating room at the time of surgery. Subject inclusion criteria were: (i) ability to provide written informed consent, (ii) 21 yr old and (iii) evolving brain lesions post SRS requiring neurosurgical resection (whether for symptomatic control or to establish pathology). Exclusion criteria were: (i) inability to undergo a MRI or PET/CT scan and (ii) pregnant or nursing female. In total, 14 patients participated in the study.

^{18}F-Fluorocholine radiosynthesis

^{18}F-Fluorocholine was manufactured at the Memorial Sloan Kettering Radiochemistry and Molecular Imaging Probe Core Facility using a fully automated radiosynthesis method on the General Electric TracerLab MX module. ^{18}F-Fluorocholine was synthesized by the ^{18}F-fluoroalkylation of N, N-dimethylaminoethanol using ^{18}F-fluorobromomethane as the fluoromethylating agent. ^{18}F-Fluorobromomethane was produced by the reaction of dibromomethane with ^{18}F-fluoride, assisted by Kryptofix 222. After purification on solid-phase extraction cartridges, the ^{18}F-Fluorocholine was obtained with >99% radiochemical purity.

PET/CT imaging

Dynamic PET scans were performed for a total of 40-min over a single field of view (15.7 cm axially) on the Discovery STE (for n=3 patients), 690 (n=4 patients) or 710 (n=7 patients) PET/CT (GE Health Care, Inc.). Dynamic scans started upon injection of 392±11 MBq of ^{18}F-Fluorocholine. Images were acquired in list mode and binned into 6×5-sec, 3×10-sec, 4×60-sec, 2×150-sec, 2×300-sec and 2×600-sec. A CT scan (120 kV, 150 mA, and 3.8-mm slice thickness) was used for attenuation correction and anatomical localization. PET emission data were acquired in 3-dimensional mode, corrected for attenuation, scatter, and random events, and iteratively reconstructed into a 256×256×47 matrix (voxel dimensions: 1.17×1.17×3.27 mm^3) using the ordered subset expectation maximization algorithm provided by the manufacturer.

Blood sample analysis

Radioactivity in whole blood and plasma specimens was radioassayed with a calibrated well counter (1480 Wallac Wizard 3 Automatic Gamma Counter (Perkin Elmer, Inc.)) [9]. Briefly, four venous blood samples were obtained at approximately 1 min, 5 min, 10 min and 30 min post-injection. Plasma radioactivity was integrated by trapezoidal method as area-under-curve. The measured radioactivity concentrations were converted to percentage injected dose per liter (%ID/L).

Image analysis

All image processing was performed in PMOD v3.604 (PMOD Software, RRID:SCR_016547). Lesions were identified by a physician with experience in nuclear medicine. Volumes of interest (VOIs) were manually drawn over the identified lesions to derive time-activity curves (TACs) and to measure the mean standardized uptake value

within the VOI corrected by body weight (SUV_{bw}). Maximum SUV values were determined on the last 10-min dynamic frame. For each patient, analysis was also performed for spherical VOIs placed over normal brain tissue (5 VOIs each with 10 mm radius). Motion correction techniques were not applied, because patient immobilization resulted in minimal motion and PET-CT mismatch.

The input function (IF) was image-derived by defining a VOI over the internal carotid artery on the early frame that allowed for the best visualization. For each patient, whole-blood IF TACs were defined using the available temporal data, corrected for partial-volume effect [10], scaled by the whole-blood activity concentration as measured from blood samples and finally corrected to account for the fraction of ^{18}F-Fluorocholine in plasma. Metabolite counts were not analyzed; instead, a population-based metabolite correction derived from ^{11}C-Choline dynamic PET studies was applied, with the percentage of activity due to unmetabolized ^{18}F-Fluorocholine being 90%, 60%, 40% and 19% at 1, 5, 10 and 30 min after injection, respectively [11,12].

Both reversible 1-compartment (1T2K) and irreversible and reversible 2-compartment (2T3K and 2T4K, respectively) pharmacokinetic models with a blood volume fraction component (v_B) were implemented to calculate kinetic rate constants K_1, k_2, k_3 and k_4. A unidirectional uptake rate constant (K_i^C) was also calculated, defined as

$$K_i^C = \frac{K_1 k_3}{k_2 + k_3} . \tag{1}$$

In addition to pharmacokinetic modeling, Patlak graphical analysis was performed to calculate net influx rate of the radiotracer (K_i^P [13,14]).

Contrast-enhanced MRI was performed before or after PET, with a mean of +/− 3 days (range 0–13). When compared to the first MRI after completion of SRS, there was a 20% increase in the median longest diameter (33 mm; range 21–61 mm). Although qualifying for progressive disease according to the proposed Response Assessment in Neuro-Oncology brain metastasis (RANO-BM) criteria [15], this change does not distinguish between viable disease vs. RN.

Histopathology

Patients were re-injected with 72±14 MBq (range, 55.5–107.3 MBq) of ^{18}F-Fluorocholine 95±26 min (range, 55–152 min) prior to surgical resection and 2±1 days (range, 1–4 days) after the ^{18}F-Fluorocholine PET. Multiple tissue samples were collected for each lesion. Each sample was placed in a separate 10% formalin-containing vials, re-weighted, and immediately counted in a calibrated Wallac gamma-ray spectrometer (located outside the operating room). Decay-corrected radioactivity of each sample was determined. Multiple samples ranging from high to low radioactivity were blindly reviewed by a neuropathologist for presence of viable tumor and necrosis content, microvascular proliferation, reactive gliosis and mono- and polymorphonuclear inflammatory infiltrates, using a semiquantitative system (scale between 0 [not a feature] and 3 [most conspicuous]). The tissue sections were

evaluated based on the percentage of viable tumor and necrosis content using 20% increments.

For each sample, ^{18}F-Fluorocholine SUV was calculated as the measured radioactivity in the sample (determined by measuring the decay-corrected net count rate and applying a calibration factor that relates the counts per minute to kBq/cc), divided by the injected activity and patient body mass.

Statistical Analysis

The correlation strength between the investigated indices was analyzed using Pearso s correlation coefficient *r*. p<0.05 was assumed to represent statistical significance. Kaplan-Meier method was implemented to visualize the survival curves of two groups of patients split based on the population median of ^{18}F-Fluorocholine PET SUV_{max}. The mean follow-up time was 31 ± 21 months (range, 2–68 months). Observations were censored if the patient was alive at the time of last follow-up or deceased from a cause other than progressing brain metastases. Log-rank test was performed to test whether the two survival curves were significantly different.

Correlation between five pathology metrics derived from resected tissue samples (i.e., viable tumor, necrosis content, microvascular proliferation, reactive gliosis and inflammatory infiltrates) and ^{18}F-Fluorocholine SUV was investigated with a linear mixed model to incorporate the random effects due to clustering (*i.e.*, each patient is a cluster), using the R package *lme4* as described previously [16]. Both univariate and multivariate regression models were run. Significant covariates in univariate analysis (p<0.05) were included in the multivariate analysis. Assigned weights for ^{18}F-Fluorocholine SUV were inversely proportional to the coefficient of variation from the decay-corrected net counts per minute. Statistical significance level of the fixed effects based on linear mixed model results was approximated by t-test with Satterthwaite degrees of freedom using the *lmerTest* package.

RESULTS

[18]F-Fluorocholine PET was performed in 14 patients with 22 treated BM between January 2014 and May 2016, including patients with lung cancer (n=3), melanoma (n=3), breast cancer (n=2), and one patient with colorectal cancer, ovarian cancer, testicular germ cell tumor, renal carcinoma, endocrine carcinoma and leiomyosarcoma (Table 1). No reactions or adverse events associated with ^{18}F-Fluorocholine were observed in any of the patients. 10 out of 12 patients in whom surgical samples were acquired exhibited pathologic recurrence. (The confirmation of RN in 2 remaining patients was determined clinically on subsequent MRI scans performed 32 and 36 months later, respectively.) For two patients, dynamic PET images could not be analyzed due to the absence of attenuation-corrected dynamic data and slow influx of activity through the major vessels into the head, possibly due to less than optimal tracer bolus. However, there were no indications of tracer extravasation at the injection site. In another two patients, research tissue samples were not acquired. 20 lesions were identified in 12 patients with evaluable PET scans, measuring 7.9 ± 8.7 cm^3 (range, 0.4–33.3 cm^3).

The percentage of activity due to ^{18}F-Fluorocholine in plasma was: 67±11%, 65±9%, 65±7% and 64±7% at 1, 5, 10 and 30 min after injection. Intratumor ^{18}F-Fluorocholine uptake reached 80% and 90% of the total activity at 3±4 and 7±6 minutes (median, 1 and 6 minutes) post injection, respectively. Total tumor ^{18}F-Fluorocholine was measured at 40 minutes. ^{18}F-Fluorocholine uptake was low in the normal brain parenchyma; average brain background SUV values were 0.2±0.1. The average SUV_{max} and SUV_{mean} for all 20 lesions studied was 6.2±3.3 and 3.0±1.8 respectively (Table 2).

According to Akaike Information Criterion (AIC), 2-tissue compartment model was preferred over 1-tissue compartment model (both including a blood component) in 16 out of 20 cases. Mean AIC values in all 20 cases were 138±44, 116±36 and 115±36 for 1C2K, 2C3K and 2C4K models, respectively. Including the blood component v_B improved the AIC values. 2T3K model resulted in lower AIC values compared to 2T4K model in 13 out of 20 cases. In the remaining 7 cases, 2T4K model was preferred due to non-negative k_4 (0.008±0.009 min^{-1}). 2C3K model resulted in lowest AIC values when fitting normal brain tissue (109±22, 105±21 and 109±21 for 1C2K, 2C3K and 2C4K models, respectively).

In lesions, Pearson's *r* between kinetic rate constants derived from whole tumor VOIs and SUV_{mean} was 0.74, 0.14 and −0.17 for K_1, k_2 and k_3, respectively (K_1 was not significantly correlated with neither k_2 nor k_3). The analysis was also repeated for small intratumor VOIs encompassing few voxels with the highest uptake of ^{18}F-Fluorocholine (i.e., highest SUV on the last dynamic frame). Corresponding Pearson's *r* between kinetic rate constants and SUV_{max} was 0.70, 0.00 and −0.01 for K_1, k_2 and k_3, respectively. Net influx rate constant as calculated with a 2C3K model, K_i^C, closely matched the corresponding metric derived from Patlak graphical analysis, K_i^P (*r*=0.98 and *r*=0.94 for mean and max, respectively). Strong correlation was observed between max K_i^C and SUV (*r*=0.83). For normal brain tissue, *r* between SUV_{mean} and K_1, k_2 and k_3 was 0.38, −0.20 and 0.17, respectively. K_1 was significantly higher in lesions compared to normal brain tissue.

^{18}F-fluorocholine PET-derived SUV_{max} was significantly correlated with the count-derived SUV from surgical samples in the most ^{18}F-fluorocholine-avid tissue sample (*r*=0.66, p<0.01; Figure 1A). Correlation with the count-derived SUV_{max} was also plotted for $K_{1,max}^C$ (Figure 1B), $K_{1,max}$ (Figure 1C) and $k_{3,max}$ (Figure 1D). Of note, neurosurgeons attempted to resect tissue samples from PET avid regions, but accurate spatial colocalization was both difficult and approximate. Mean SUV across all tissue samples in a lesion was 4.8±2.6, whereas SUV_{max} for the hottest tissue sample per lesion was 7.8±4.1. Correlations were also calculated between $K_{i.max}$, and $K_{1,max}$ and the static SUV_{max}. (Figure 2A, 2B), highlighting that ^{18}F-fluorocholine uptake at 40-min post-injection is primarily dependent on K_1. As expected, K_i^P and K_i^C were also found to be highly correlated (*r* = 0.94, p<0.01; Figure 2C).

113 surgical samples were collected from 14 resected lesions in 12 patients (8±4 per lesion; weighing 0.16±0.12 g). 10 out of 14 lesions (in 10 out of 12 patients) were positive for tumor recurrence, whereas the remaining 4 out of 14 lesions were negative. In 10 lesions positive for tumor recurrence, 76±34% of samples were positive (range, 9–100%). In total, evidence of viable tumor was present on 69 samples (61%) while 83 (76%) had necrosis,

with 57 samples (53%) containing both. 58 samples (55%) were positive for vascular proliferation, 61 (55%) had gliosis, and 45 (41%) had inflammation (not all 113 samples were scored for all). Mean tumor and necrosis content, averaged over all samples from the same lesion, were 29%±27% (range, 0–80%) and 23%±17% (range, 0–42%), respectively. Mean semiquantitative values for microvascular proliferation, mononuclear and polymorphonuclear inflammatory infiltrates and reactive gliosis (scale between 0 and 3) were 0.5±0.4, 0.6±0.7 and 0.5±0.4, respectively. Surgical samples with viable tumor had higher ^{18}F-fluorocholine uptake than those without tumor (SUV of 4.5±3.7 compared to 2.6±3.0; p=0.01). The analysis with a linear mixed model revealed that ^{18}F-fluorocholine uptake in the surgical samples was driven by the degree of reactive gliosis (p=0.011) and inflammation (p=0.021); a multivariate regression analysis showed a significant correlation between resection tissue ^{18}F-Fluorocholine SUV and reactive gliosis (p=0.011), viable tumor (p=0.015) and inflammation (p=0.022). No correlation of ^{18}F-fluorocholine uptake with proliferation and percentage necrosis was observed based on both analyses. There was no significant correlation between ^{18}F-Fluorocholine SUV and sample processing time post-injection (r=0.07) or sample net weight (r=0.08).

^{18}F-Fluorocholine SUV$_{max}$ as a function of follow-up time is presented in Figure 3A (date of last follow-up: October 7th, 2019). The data was split into two groups according to median ^{18}F-fluorocholine SUV$_{max}$ value of 6. Survival distributions were visualized with Kaplan-Meier estimators (Figure 3B). Patients with ^{18}F-Fluorocholine SUV$_{max}$ above the median value of 6 had worse prognosis, however significance was not reached (log-rank test, p=0.068). Observations were censored if the patient was alive at the time of last follow-up (blue diamonds on Fig. 3A) or deceased from cause other than progressing brain metastases (orange square on Fig. 3A).

^{18}F-Fluorocholine PET/CT images together with tumor time-activity curves and surgical samples are shown for two representative patients with (Fig. 4) and without (Fig. 5) pathologic confirmation of tumor recurrence, illustrating different ^{18}F-Fluorocholine pharmacokinetics between lesions

DISCUSSION

The aim of the current study was to determine whether PET imaging with ^{18}F-Fluorocholine reliably discriminates between RN and tumor recurrence. For that purpose, we performed ^{18}F-Fluorocholine dynamic PET scans in patients with radiographic changes requiring surgery after SRS for BM. Our cohort was skewed, as 10 out of 14 patients exhibited pathologic recurrence. PET-derived ^{18}F-Fluorocholine SUV$_{max}$ was significantly correlated with uptake in the most ^{18}F-Fluorocholine-avid surgical sample. While the radiographic and outcome analyses are underpowered due to paucity of events, our results indicate that ^{18}F-Fluorocholine may reflect the presence of viable tumor in patients with radiologic progression after SRS on microscopic (i.e., specimen activity) as well as macroscopic (i.e., PET) measures. Additionally, ^{18}F-Fluorocholine PET SUV$_{max}$ appears to allow for the identification of patients that have increased risk of death due to progressing brain metastases. Of note, in addition to percentage viable tumor, inflammation and reactive gliosis also resulted in elevated ^{18}F-Fluorocholine SUV in resected tissue samples.

Other PET radiotracers have been investigated for differentiating tumor recurrence from radionecrosis in brain. ^{18}F-Fluorodeoxyglucose (FDG) is avidly accumulated in inflammatory regions where white blood cells and macrophages have high rates of glycolysis. The high background level of FDG in normal brain tissue compromises its ability to distinguish progressive disease and consequently FDG PET is not widely utilized for this purpose. The sensitivity and specificity of ^{18}F-FDG PET to distinguish recurrent tumor from radiation necrosis was reported to be in the range of 65–86% and 22–94%, respectively [17–19]. On the other hand, radiolabeled amino acids such as ^{11}C-methionine and O-(2-^{18}F-fluoroethyl)-L-tyrosine (^{18}F-FET) have relatively high tumor and low brain uptake, with studies showing promising results in differentiating RN from tumor recurrence in brain metastases [20, 21]. However, normal brain uptake of the amino acids was reported to be higher than that of ^{18}F-Fluorocholine. Tumor uptake of ^{11}C-Choline and ^{18}F-Fluorocholine has been shown to be greater than ^{11}C-methionine and other amino acids [22]. In a direct comparison of ^{11}C-methionine with ^{11}C-choline, Rottenburger et al. concluded that ^{11}C-choline is a promising radiotracer for the imaging of brain metastases compared with ^{11}C-methionine due to significantly higher tumor-to-blood ratios, without evidence for a lower specificity of ^{11}C-choline uptake [23]. These findings are expected to be translatable to ^{18}F-substituted choline analogs due to similar tumor uptake patterns [24]. Recent reports indicate that metabolic imaging with 6-^{18}F-fluoro-L-dopa (^{18}F-FDOPA) PET and analysis of semiquantitative uptake indices is a promising tool for differentiating recurrent or progressive brain metastases from late or delayed radiation injury [25,26]. To best of our knowledge, a direct comparison study between ^{18}F-Fluorocholine and ^{18}F-FDOPA has not been performed.

Another goal of our study was to determine whether pharmacokinetic modeling of ^{18}F-Fluorocholine uptake from dynamic PET acquisitions adds benefit, as has been shown for ^{18}F-FET [20] and a-[11]Cmethyl-L-tryptophan [27]. In our study, a high correlation was observed between SUV and the net uptake rate constant K_i. This observation supports the use of static SUV at later times (e.g. 40 min) post injection, once tumor uptake has plateaued. ^{18}F-Fluorocholine uptake was rapid and sustained, as observed previously [12, 29–31] and appears to reach a plateau faster than ^{18}F-FET [32]. In the irreversible 2-compartment model, the K_1 term may incorporate some of the "trapping" component (e.g., transport into tumor cells, rapid phosphorylation, etc.), in addition to lesion perfusion and vascular permeability. Since phosphorylation of choline is rapid [33], it may not be accurately identified as "k_3" in the kinetic model. Although the k_3 term is justified based on Akaike Information Criterion and reflects a slower process, it was not correlated with ^{18}F-Fluorocholine SUV_{max} in the PET images. However, in a comparison between surgical samples and PET imaging metrics, k_3 estimates and surgical sample-derived SUV_{max} values were correlated, although the PET voxels and surgical sample were not spatially colocalized with certainty.

In this cohort of patients, ^{18}F-Fluorocholine uptake at 40-min post-injection is primarily driven by K_1, as indicated by the differences between lesions with and without pathologic evidence of tumor as well as by the high correlation between K_1 and SUV in lesions and the absence of corresponding correlation between k_3 and SUV. Others have noted that ^{18}F-Fluorocholine K_1 and k_3 may not be physiologically identifiable. The non-negative k_3 values

in brain may reflect choline uptake that is utilized for synthesis of the neurotransmitter acetylcholine (^{18}F-Fluorocholine SUV in normal brain increased by about 6–8% during the second half of the 40-min dynamic acquisition); however, accurate estimation of k_3 in normal brain is compromised due to relatively low K_1. Furthermore, a limitation of our analysis is that a population-based metabolite correction was used, derived from ^{11}C-Choline data [11,12]. Bansal and colleagues concluded that ^{18}F-Fluorocholine mimics radiolabeled choline as a biochemical tracer, although metabolic rates to both lipid and oxidative metabolites were moderately attenuated for ^{18}F-Fluorocholine relative to ^{14}C-choline [33]. The same group reported that a small but appreciable fraction of ^{18}F-Fluorobetaine (a metabolite of ^{18}F-Fluorocholine) was observed in tumors of glioma-bearing rats [33], whereas the implemented pharmacokinetic model assumes that ^{18}F-Fluorobetaine is not significantly accumulated in tumors. Slaets and colleagues concluded that the blood metabolism of ^{11}C-Choline and ^{18}F-Fluorocholine were similar in mice and that corrections for ^{18}F-Fluorobetaine uptake were not mandatory [34]. When our analysis was repeated with a 3-compartment pharmacokinetic model with two input functions that accounts for non-specific uptake of radiometabolites (Supplementary Table S1), similar values were observed for K_1, k_2 and k_3.

CONCLUSIONS

This is the first study to our knowledge in which the PET radiotracer ^{18}F-Fluorocholine was injected peri-operatively, allowing radiotracer uptake to be correlated with pathologic diagnosis in tissue samples obtained at surgery. Our findings suggest that ^{18}F-Fluorocholine PET SUV correlates with pathologic evidence of recurrent tumor after SRS for BM. The strong correlation between ^{18}F-Fluorocholine SUV and the net influx rate (K_i) supports the use of a simpler static PET acquisition, instead of requiring a dynamic or a dual-phase acquisition.

Supplementary Material

Refer to Web version on PubMed Central for supplementary material.

Acknowledgments

REFERENCES

1. Nayak L, Lee EQ and Wen PY. Epidemiology of brain metastases. Curr Oncol Rep. 2012;14:48–54. [PubMed: 22012633]

2. Patchell RA. The management of brain metastases. Cancer Treat Rev. 2003;29:533–40. [PubMed: 14585263]

3. Kohutek ZA, Yamada Y, Chan TA, et al. Long-term risk of radionecrosis and imaging changes after stereotactic radiosurgery for brain metastases. J Neurooncol. 2015;125:149–56. [PubMed: 26307446]

4. Heper AO, Erden E, Savas A, et al. An analysis of stereotactic biopsy of brain tumors and nonneoplastic lesions: a prospective clinicopathologic study. Surg Neurol. 2005;64:S82–8. [PubMed: 16256850]

5. Kongkham PN, Knifed E, Tamber MS and Bernstein M. Complications in 622 cases of frame-based stereotactic biopsy, a decreasing procedure. Can J Neurol Sci. 2008;35:79–84. [PubMed: 18380282]

6. DeGrado TR, Coleman RE, Wang S, et al. Synthesis and evaluation of 18F-labeled choline as an oncologic tracer for positron emission tomography: initial findings in prostate cancer. Cancer Res. 2001;61:110–7. [PubMed: 11196147]

7. DeGrado TR, Reiman RE, Price DT, Wang S and Coleman RE. Pharmacokinetics and radiation dosimetry of 18F-fluorocholine. J Nucl Med. 2002;43:92–6. [PubMed: 11801711]

8. Kwee SA, Ko JP, Jiang CS, Watters MR and Coel MN. Solitary brain lesions enhancing at MR imaging: evaluation with fluorine 18 fluorocholine PET. Radiology. 2007;244:557–65. [PubMed: 17581887]

9. Dunphy MPS, Harding JJ, Venneti S, et al. In Vivo PET Assay of Tumor Glutamine Flux and Metabolism: In-Human Trial of 18F-(2S,4R)-4-Fluoroglutamine. Radiology. 2018;287:667–75. [PubMed: 29388903]

10. Grkovski M, Schwartz J, Gönen M, et al. Feasibility of 18F-Fluoromisonidazole Kinetic Modeling in Head and Neck Cancer Using Shortened Acquisition Times. J Nucl Med 2016;57:334–341. [PubMed: 26609178]

11. Roivainen A, Forsback S, Grönroos T, et al. Blood metabolism of [methyl-^{11}C]choline; implications for in vivo imaging with positron emission tomography. Eur J Nucl Med. 2000;27:25–32. [PubMed: 10654143]

12. Kenny LM, Contractor KB, Hinz R, et al. Reproducibility of [^{11}C]choline-positron emission tomography and effect of trastuzumab. Clin Cancer Res. 2010;16:4236–45. [PubMed: 20682702]

13. Patlak CS, Blasberg RG and Fenstermacher JD. Graphical evaluation of blood-to-brain transfer constants from multiple-time uptake data. J Cereb Blood Flow Metab. 1983;3:1–7. [PubMed: 6822610]

14. Patlak CS and Blasberg RG. Graphical evaluation of blood-to-brain transfer constants from multiple-time uptake data. Generalizations. J Cereb Blood Flow Metab. 1985;5:584–90. [PubMed: 4055928]

15. Lin NU, Lee EQ, Aoyama H, et al. Response assessment criteria for brain metastases: proposal from the RANO group. Lancet Oncol. 2015;16:e270–8. [PubMed: 26065612]

16. Huguet F, Yorke ED, Davidson M, et al. Modeling pancreatic tumor motion using 4-dimensional computed tomography and surrogate markers. Int J Radiat Oncol Biol Phys. 2015;91:579–87. [PubMed: 25680600]

17. Ricci PE, Karis JP, Heiserman JE, Fram EK, Bice AN and Drayer BP. Differentiating recurrent tumor from radiation necrosis: time for re-evaluation of positron emission tomography? AJNR Am J Neuroradiol. 1998;19:407–13. [PubMed: 9541290]

18. Langleben DD and Segall GM. PET in differentiation of recurrent brain tumor from radiation injury. J Nucl Med. 2000;41:1861–7. [PubMed: 11079496]

19. Chao ST, Suh JH, Raja S, Lee SY and Barnett G. The sensitivity and specificity of FDG PET in distinguishing recurrent brain tumor from radionecrosis in patients treated with stereotactic radiosurgery. Int J Cancer. 2001;96:191–7. [PubMed: 11410888]

20. Galldiks N, Stoffels G, Filss CP, et al. Role of O-(2-(18)F-fluoroethyl)-L-tyrosine PET for differentiation of local recurrent brain metastasis from radiation necrosis. J Nucl Med. 2012;53:1367–74. [PubMed: 22872742]

21. Terakawa Y, Tsuyuguchi N, Iwai Y, et al. Diagnostic accuracy of 11C-methionine PET for differentiation of recurrent brain tumors from radiation necrosis after radiotherapy. J Nucl Med. 2008; 49:694–9. [PubMed: 18413375]

22. Sollini M, Sghedoni R, Erba PA, et al. Diagnostic performances of [18F]fluorocholine positron emission tomography in brain tumors. Q J Nucl Med Mol Imaging. 2018;62:209–19. [PubMed: 26329494]

23. Rottenburger C, Hentschel M, Kelly T, et al. Comparison of C-11 methionine and C-11 choline for PET imaging of brain metastases: a prospective pilot study. Clin Nucl Med. 2011;36:639–42. [PubMed: 21716012]

24. Hara T 11C-choline and 2-deoxy-2-[18F]fluoro-D-glucose in tumor imaging with positron emission tomography. Mol Imaging Biol. 2002;4:267–73. [PubMed: 14537115]

25. Lizarraga KJ, Allen-Auerbach M, Czernin J, et al. (18)F-FDOPA PET for differentiating recurrent or progressive brain metastatic tumors from late or delayed radiation injury after radiation treatment. J Nucl Med. 2014;55:30–6. [PubMed: 24167081]

26. Cicone F, Minniti G, Romano A, et al. Accuracy of F-DOPA PET and perfusion-MRI for differentiating radionecrotic from progressive brain metastases after radiosurgery. Eur J Nucl Med Mol Imaging. 2015;42:103–11. [PubMed: 25182751]

27. Alkonyi B, Barger GR, Mittal S, et al. Accurate differentiation of recurrent gliomas from radiation injury by kinetic analysis of α−11C-methyl-L-tryptophan PET. J Nucl Med. 2012;53:1058–64. [PubMed: 22653792]

28. Kelly T, et al. Comparison of C-11 methionine and C-11 choline for PET imaging of brain metastases: a prospective pilot study. Clin Nucl Med. 2011;36:639–42 [PubMed: 21716012]

29. Sutinen E, Nurmi M, Roivainen A, et al. Kinetics of [(11)C]choline uptake in prostate cancer: a PET study. Eur J Nucl Med Mol Imaging. 2004;31:317–24. [PubMed: 14628097]

30. Schaefferkoetter JD, Wang Z, Stephenson MC, et al. Quantitative ^{18}F-fluorocholine positron emission tomography for prostate cancer: correlation between kinetic parameters and Gleason scoring. EJNMMI Res. 2017;7:25. [PubMed: 28324340]

31. Grkovski M, Gharzeddine K, Sawan P, et al. ^{11}C-Choline Pharmacokinetics in Recurrent Prostate Cancer. J Nucl Med. 2018;59:1672–8. [PubMed: 29626123]

32. Lohmann P, Herzog H, Rota Kops E, et al. Dual-time-point O-(2-[(18)F]fluoroethyl)-L-tyrosine PET for grading of cerebral gliomas. Eur Radiol. 2015;25:3017–24. [PubMed: 25813014]

33. Bansal A, Shuyan W, Hara T, Harris RA and Degrado TR. Biodisposition and metabolism of [(18)F]fluorocholine in 9L glioma cells and 9L glioma-bearing fisher rats. Eur J Nucl Med Mol Imaging. 2008;35:1192–203. [PubMed: 18264706]

34. Slaets D and De Vos F. Comparison between kinetic modelling and graphical analysis for the quantification of [18F]fluoromethylcholine uptake in mice. EJNMMI Res. 2013;3:66. [PubMed: 24034278]
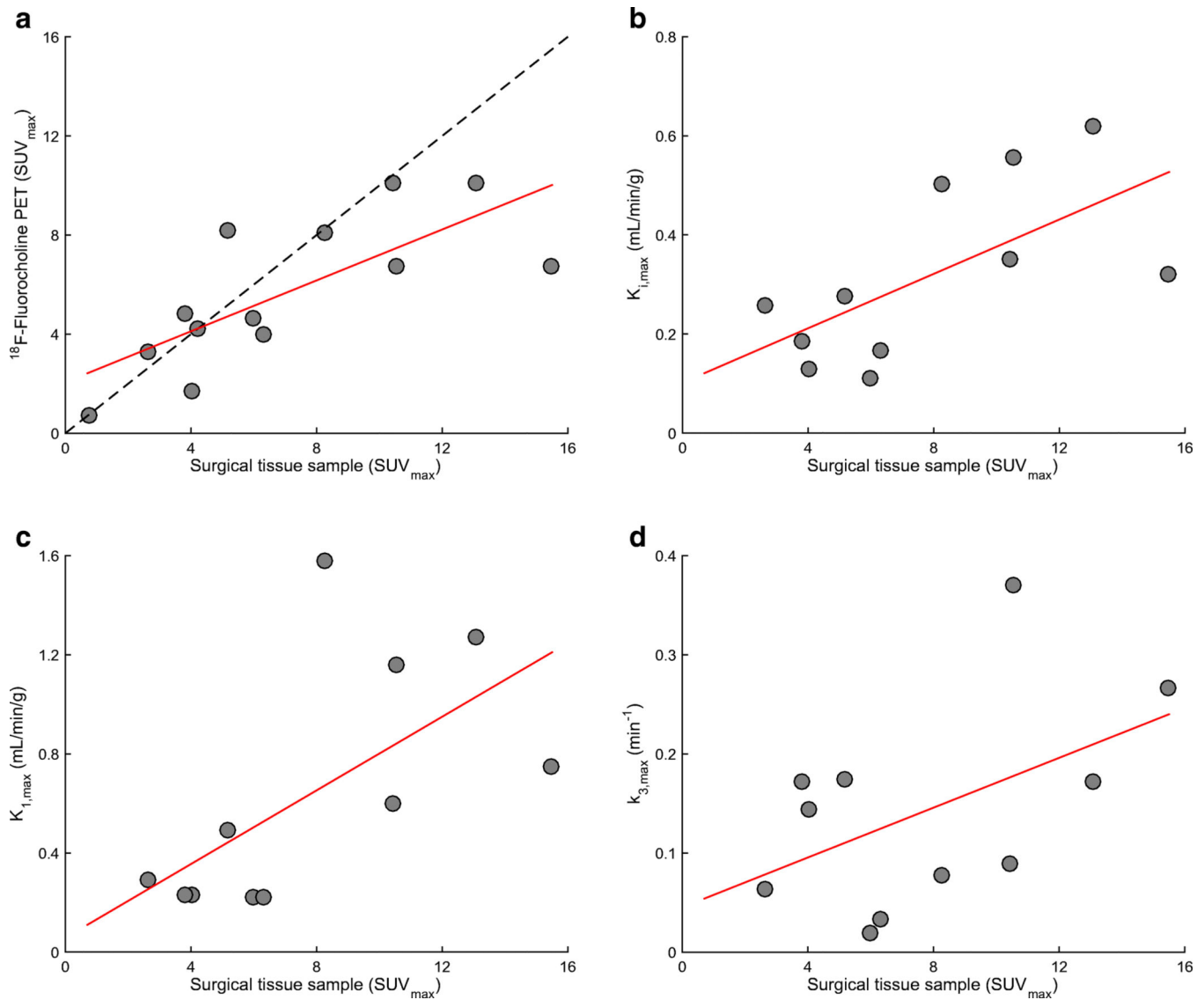
Figure 1.

Correlation between ^{18}F-Fluorocholine uptake in surgical samples and PET imaging metrics. (A) ^{18}F-Fluorocholine SUV$_{max}$ as measured from a surgically removed sample with highest uptake (one sample per patient, 95±28 min post-injection) and by PET (single voxel with highest uptake, 30–40 min post-injection), with superimposed identity (dashed grey) and regression (solid red) lines; Pearson's r=0.66. Data is derived from n=13 lesions for which both sets of information was available, including two patients for which dynamic ^{18}F-Fluorocholine could not be analyzed. Of note, PET voxel and sample might not be spatially colocalized. (B) Scatterplot of ^{18}F-Fluorocholine $K_{i,max}{}^C$ and SUV$_{max}$ as measured from a surgically removed sample with highest uptake. n=11 lesions; $r = 0.65$. (C) Corresponding scatterplot for ^{18}F-Fluorocholine $K_{1,max}$; $r = 0.63$. (D) Corresponding scatterplot for ^{18}F-Fluorocholine $k_{3,max}$; $r = 0.50$.
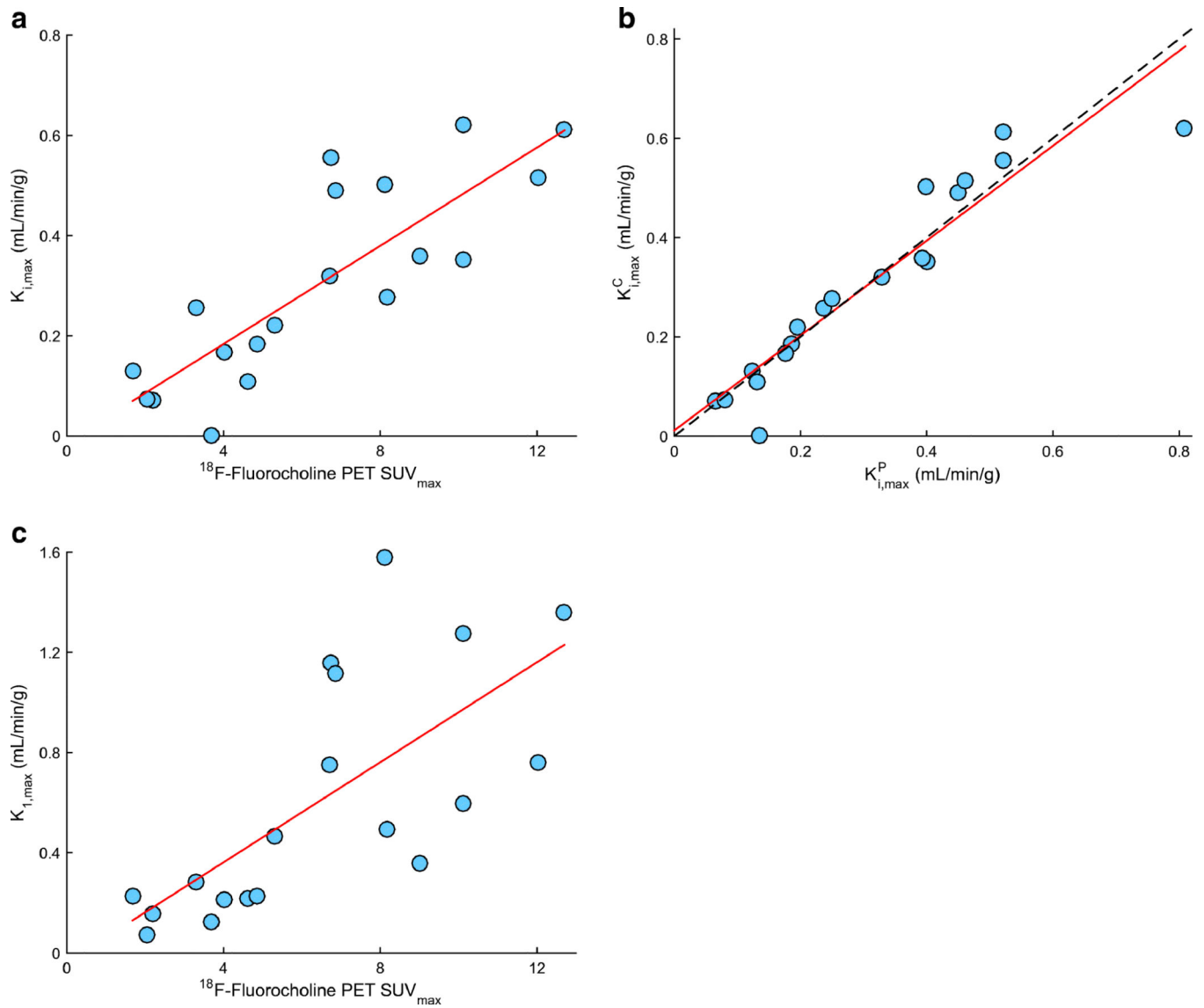
Figure 2.
Correlation between investigated ^{18}F-Fluorocholine PET imaging metrics in n=19 lesions for which pharmacokinetic modeling was performed. Regions of interest were focused on the are with highest uptake of ^{18}F-Fluorocholine. (A) PET SUV_{max} vs $K_{i,max}^C$; Spearman's $r = 0.83$ (p<0.01). (B) PET SUV_{max} vs K_1; $r = 0.70$ (p<0.01). (C) K_i^P vs K_i^C, with superimposed identity (dashed grey) and regression (solid red) lines; $r = 0.94$ (p<0.01).
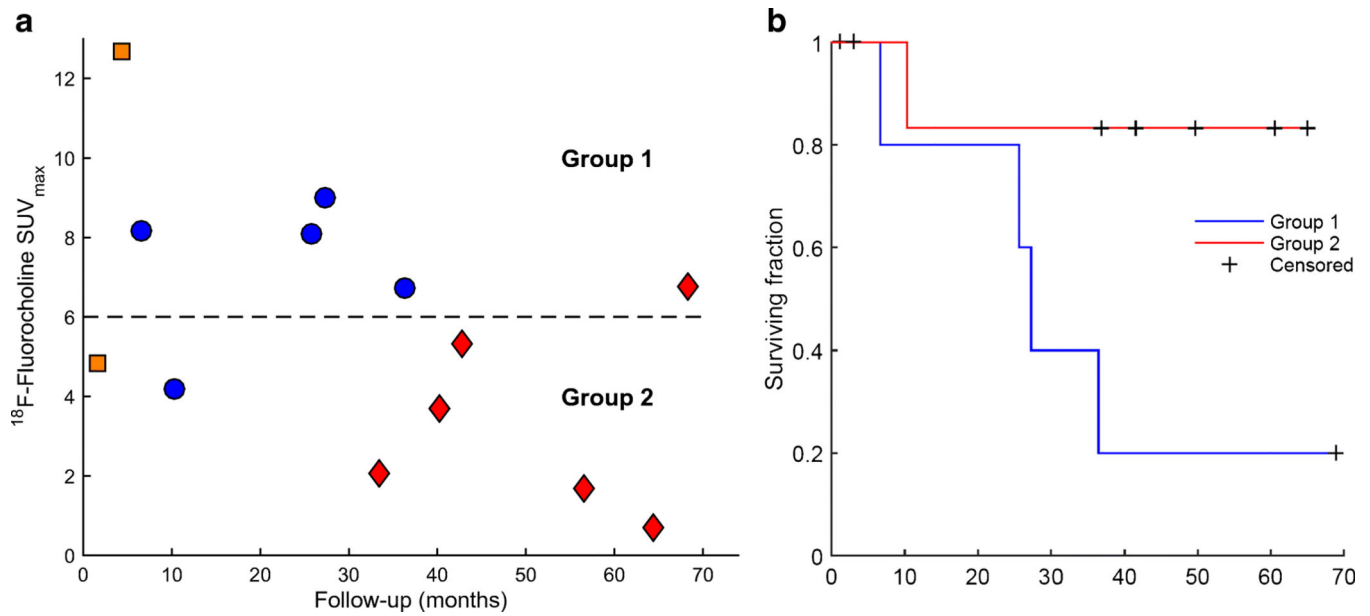
Figure 3.
(A) ^{18}F-Fluorocholine PET SUV$_{max}$ as a function of follow-up time for n=13 pts (follow-up was not established for one international patient). Blue circles - deceased from previously treated progressing brain metastases (n=5). Orange square - deceased from progressing metastases in the liver and pancreas (n=1) and previously untreated brain metastases (n=1). Red diamonds - alive (n=6). Dashed line represents ^{18}F-Fluorocholine PET SUV$_{max}$ = 6 (median value), splitting the data into two groups. (B) Kaplan-Meier estimator for groups 1 and 2. Observations were censored if the patient was alive at the time of last follow-up or deceased from cause other than progression in the treated brain metastases. Difference in survival distributions did not reach significance according to the log-rank test (p=0.068).
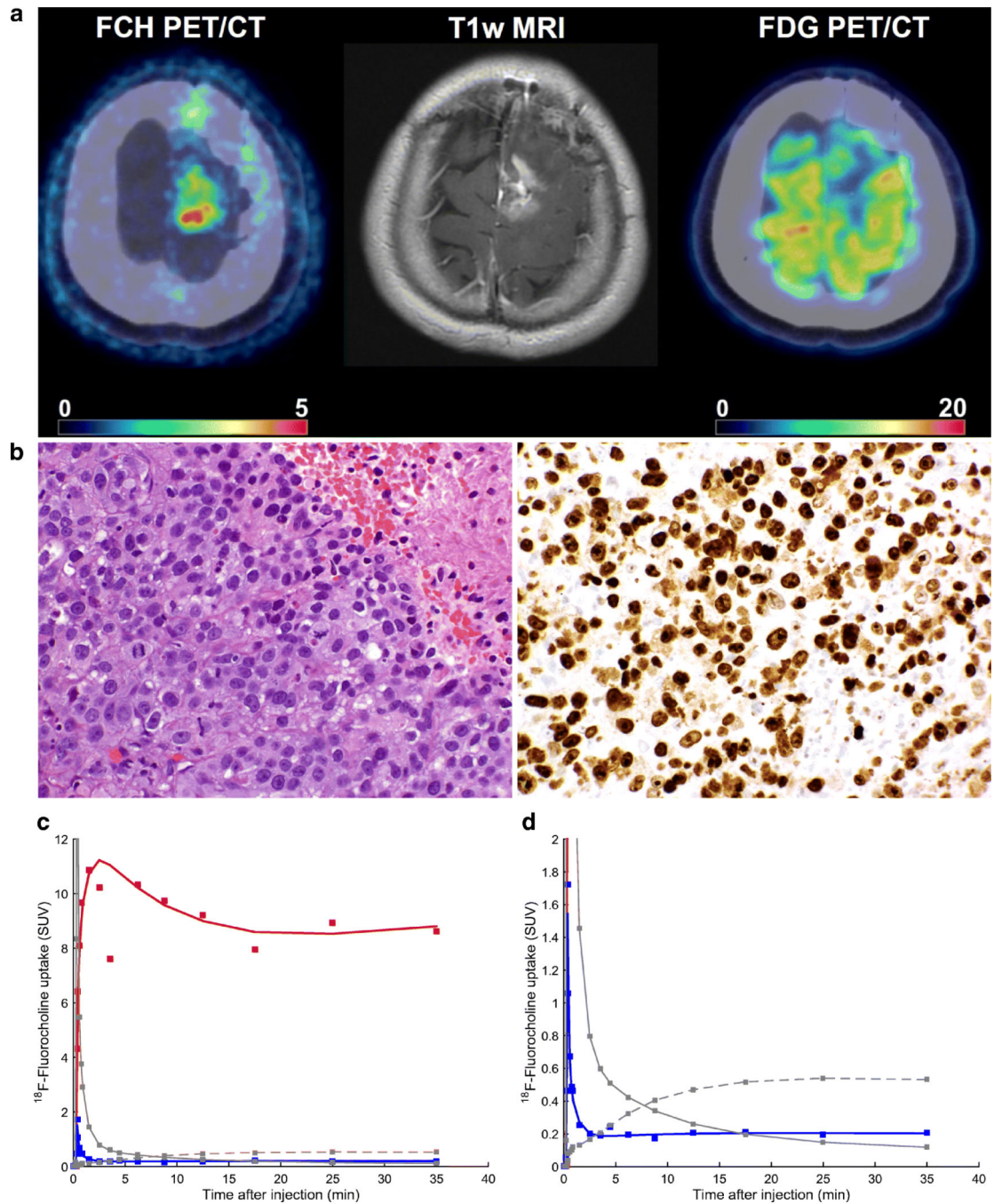
Figure 4.
[18]F-Fluorocholine PET for a lung cancer patient with pathological confirmation of recurrent tumor. (A) Axial view of the last dynamic PET frame (10-min acquisition time, 30–40 min post-injection), fused with corresponding CT, showing the 11 cm[3] metastatic lung adenocarcinoma in superior-anterior left frontal resection cavity with PET-derived SUV_{max} of 10.1. Post-Gadolinium contrast T1-weighted MRI and ^{18}F-FDG PET are included for comparison. Color bar scale are in units of SUV_{bw}. (B) Photomicrograph on the left panel shows metastatic carcinoma with focus of necrosis at upper right. Hematoxylin-eosin, 40x

magnification. Right panel shows Ki-67 staining with a proliferative index of 90%. In total, 12 surgical samples were analyzed for this patient. All of them indicated recurrent tumor and the presence of necrosis. Highest SUV_{max} was 13.1. (C) Time-activity curve for intratumor area of highest ^{18}F-Fluorocholine uptake (red). SUV, v_B, K_1, k_2, k_3 and K_i^P were 8.8, 0.04, 1.27 mL/min/g, 0.18 min^{-1}, 0.17 min^{-1} and 0.81 mL/min/g, respectively. Corresponding values for normal brain tissue were 0.2, 0.06, 0.02 mL/min/g, 0.13 min^{-1}, 0.13 min^{-1} and 0.01 mL/min/g, respectively (TAC showed in blue). Unmetabolized and metabolized ^{18}F-Fluorocholine in plasma are shown as solid and dashed grey lines, respectively. (D) Insert from panel (C), highlighting the normal brain uptake and ^{18}F-Fluorocholine activity in plasma.
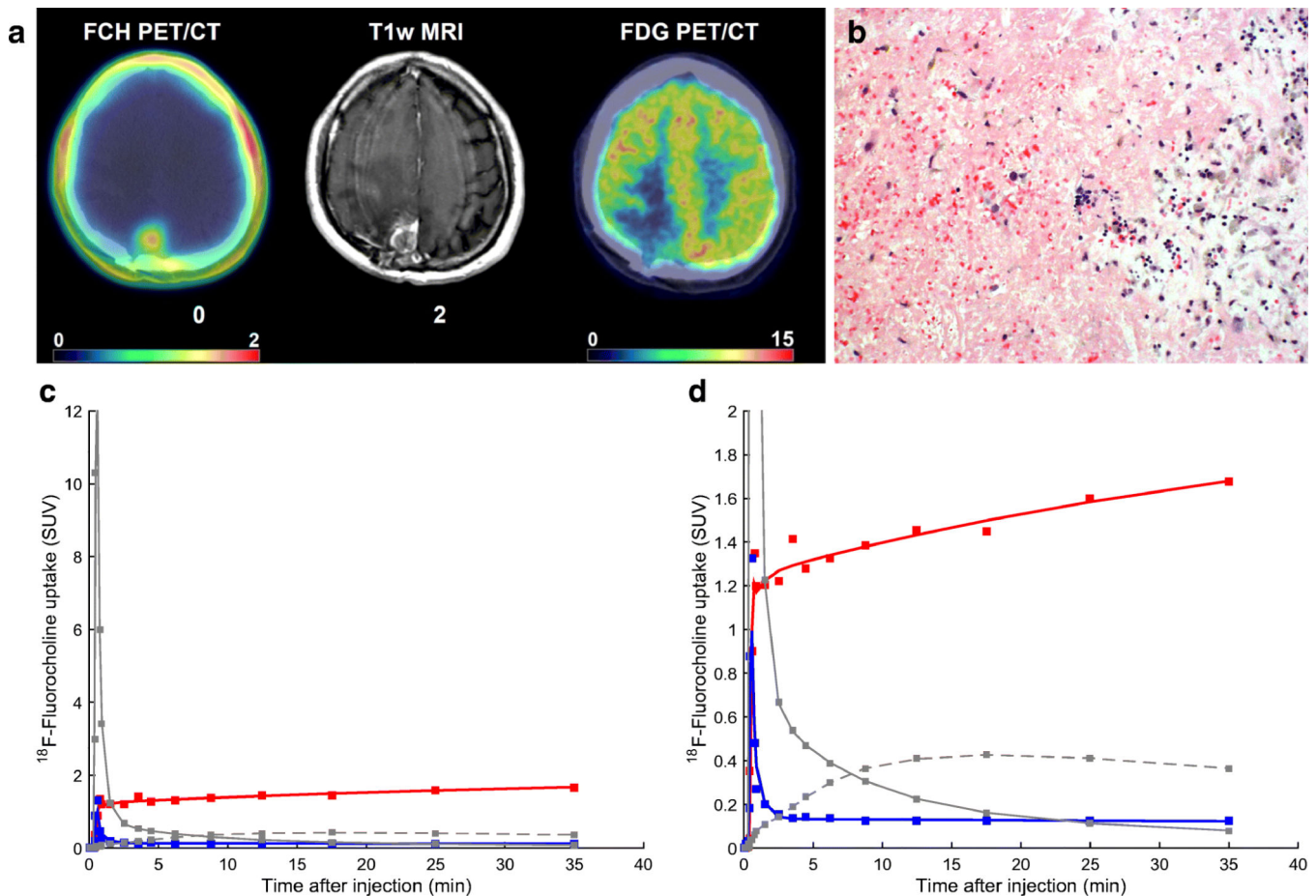
Figure 5.
[18]F-Fluorocholine PET for a lung cancer patient with no recurrent tumor seen in the surgical samples. (A) Axial view of the last dynamic PET frame (10-min acquisition time, 30–40 min post-injection), fused with corresponding CT, showing the 1.4 cm^3 lesion in paramedian right parietal lobe that was suspicious for viable tumor. PET-derived SUV$_{max}$ was 1.7. Post-Gadolinium contrast T1-weighted MRI and ^{18}F-FDG PET are shown for comparison. (B) The left half of the photomicrograph exhibits necrotic neuroparenchyma with fibrinous exudates. Seen in the right half are a few reactive lymphocytes and siderophages. Hematoxylin-eosin, 40x magnification. In total, 12 samples were analyzed for this patient. None of them indicated recurrent tumor, whereas necrosis was detectable in 7 out of 12 tissue samples. No evidence of proliferation was noted. Highest SUV$_{max}$ derived from samples was 4.0. (C) Time-activity curve for intratumor area of highest ^{18}F-Fluorocholine uptake (red). SUV, v_B, K_1, k_2, k_3 and K_i^P were 1.7, 0.06, 0.23 mL/min/g, 0.11 min^{-1}, 0.14 min^{-1} and 0.13 mL/min/g, respectively. Corresponding values for normal brain tissue were 0.1, 0.07, 0.02 mL/min/g, 0.23 min^{-1}, 0.17 min^{-1} and 0.01 mL/min/g, respectively (TAC shown in blue). Unmetabolized and metabolized ^{18}F-Fluorocholine in plasma are shown as solid and dashed grey lines, respectively. (D) Insert from panel (C), highlighting the normal brain uptake and ^{18}F-Fluorocholine activity in plasma.

Table 1.

Patient demographics.

Patient no.	Sex	Age (y)	Clinical statement	No of PET lesions in the brain	Localization	FCH SUV_{max}	Pathology	Outcome (months)	Corticosteroid use
1	F	60	Melanoma	2	L frontal	6.8	positive	AWD (68)	No
2	M	46	Lung cancer	2	L frontal	10.1	positive	unknown[†]	No
3	F	45	Breast cancer	1	L posterior parietal	6.7	positive	deceased (36)	No
4	M	50	Lung cancer	1	Paramedian R parietal	1.7	negative	AWD (57)	No
5	F	66	Ovarian cancer	1	Cerebellum	8.1	positive	deceased (26)	No
6	F	55	Endocrine carcinoma	3	Anterior R frontal, R occipital, L basal ganglia	8.2	positive	deceased (7)	Fluticasone
7	M	70	Colorectal cancer	3	R occipital	12.7	positive	deceased (4)	No
8	M	62	Lung cancer	1	L frontal	2.1	negative	AWD (33)	No
9	M	76	Renal carcinoma	1	L frontoparietal	4.8	positive	deceased (2)	Prednisone
10	M	71	Melanoma	2	L posterior parietal, R temporal	5.3	N/A[*]	AWD (43)	No
11	F	24	Leiomyosarcoma	2	R temporal, L parietal	9.0	positive	deceased (27)	Dexamethasone
12	M	22	Testicular cancer	1	R frontal	3.7	N/A[*]	AWD (40)	Dexamethasone
13	F	74	Melanoma	1	R temporal	0.7	positive[‡]	AWD (64)	No
14	F	49	Breast Cancer	1	L parietal	4.2	positive[§]	deceased (10)	No

PET - Positron emission tomography; FCH - ^{18}F-Fluorocholine; AWD - alive with disease;

[*] surgical samples were not acquired.

[†] - international patient.

[‡] - Kinetic modeling not be performed (absence of attenuation-corrected dynamic data).

[§] - Kinetic modeling not performed (slow influx of activity through the major vessels into the head, possibly due to less than optimal tracer bolus).

Table 2.

Summary of metrics derived from intratumor region of interest with highest uptake of ^{18}F-Fluorocholine. Mean ± standard deviation (range).

	All lesions (n=20)	Lesions with pathologic evidence of tumor (n=8[*])	Lesions with pathologic evidence of no tumor (n=4)	Normal brain (n=12)
SUV_{max}	6.2±3.3 (1.7±12.7)	7.2±2.1 (4.0–10.1)	2.9±1.3 (1.7–4.6)	0.2±0.01 (0.1–0.3)
$K_{i,}^{P}$ (mL/min/g)	0.30±0.19 (0.07–0.81)	0.38±0.21 (0.18–0.81)	0.14±0.07 (0.08–0.24)	0.008±0.002 (0.005–0.011)
K_{i}^{C} (mL/min/g)	0.31±0.19 (0.07–0.62)	0.34±0.19 (0.07–0.62)	0.14±0.08 (0.07–0.26)	0.006±0.003 (0.000–0.009)
v_B	0.07±0.06 (0.01–0.19)	0.07±0.06 (0.01–0.18)	0.06±0.04 (0.02–0.12)	0.04±0.02 (0.02–0.07)
K_1 (mL/min/g)	0.60±0.48 (0.07–1.58)	0.71±0.53 (0.07–1.58)	0.20±0.09 (0.07–0.29)	0.01±0.01 (0.01–0.02)
k_2 (min^{-1})	0.14±0.15 (0.01–0.54)	0.15±0.15 (0.01–0.40)	0.03±0.05 (0.01–0.11)	0.04±0.06 (0.01–0.20)
k_3 (min^{-1})	0.17±0.18 (0.01–0.76)	0.15±0.12 (0.01–0.37)	0.06±0.06 (0.01–0.14)	0.08±0.07 (0.00–0.16)

[*] For two patients with pathologic evidence of tumor, kinetic modeling could not be performed.